Environmental Science & Technology

Article

pubs.acs.org/est

An Iodide-Adduct High-Resolution Time-of-Flight Chemical-Ionization Mass Spectrometer: Application to Atmospheric Inorganic and Organic Compounds

Ben H. Lee,[†,⊥] Felipe D. Lopez-Hilfiker,[⊥,†] Claudia Mohr,[†] Theo Kurtén,[‡] Douglas R. Worsnop,[§,∥] and Joel A. Thornton*[,†]

[†]Department of Atmospheric Sciences, University of Washington Seattle, Washington 98195, United States

[‡]Department of Chemistry, University of Helsinki Helsinki, Finland

[§]Department of Physics Division of Atmospheric Sciences, University of Helsinki, Helsinki, Finland

[∥]Aerodyne Research, Inc., 45 Manning Rd., Billerica, Massachusetts 01821, United States

Supporting Information

ABSTRACT: A high-resolution time-of-flight chemical-ionization mass spectrometer (HR-ToF-CIMS) using Iodide-adducts has been characterized and deployed in several laboratory and field studies to measure a suite of organic and inorganic atmospheric species. The large negative mass defect of Iodide, combined with soft ionization and the high mass-accuracy (<20 ppm) and mass-resolving power (R > 5500) of the time-of-flight mass spectrometer, provides an additional degree of separation and allows for the determination of elemental compositions for the vast majority of detected ions. Laboratory characterization reveals Iodide-adduct ionization generally exhibits increasing sensitivity toward more polar or acidic volatile organic compounds. Simultaneous retrieval of a wide range of mass-to-charge ratios (m/Q from 25 to 625 Th) at a high frequency (>1 Hz) provides a comprehensive view of atmospheric oxidative chemistry, particularly when sampling rapidly evolving plumes from fast moving platforms like an aircraft. We present the sampling protocol, detection limits and observations from the first aircraft deployment for an instrument of this type, which took place aboard the NOAA WP-3D aircraft during the Southeast Nexus (SENEX) 2013 field campaign.

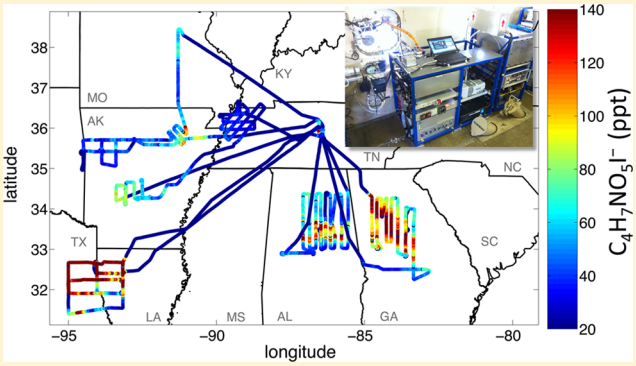

1. INTRODUCTION

Observational capabilities for atmospheric gas-phase composition remain incomplete, with implications for the accurate simulation of air quality and climate change. Several aspects of oxidative processing and subsequent particle formation and growth remain to be tested or more fully explored with observations.[1−3] Broad classes of reactive trace gases such as radical intermediates, molecular halogens and oxygenated volatile organic compounds (oVOCs) remain analytical challenges.[4−6] Negative-ion chemical ionization mass spectrometry (CIMS) represents one general approach capable of quantifying various classes of oVOCs and inorganic radicals.[7,8]

The general benefits of CIMS approaches include (1) linearity and reproducibility, (2) minimal sample preparation and handling, allowing for the measurement of highly functionalized low-volatility or reactive compounds, (3) high sensitivity combined with selectivity, and (4) high time resolution. The drawbacks of CIMS for atmospheric measurements have generally been related to the stability of the resulting molecular analyte ions, that is, ionization-induced fragmentation, and an inability to resolve structural isomers or isobaric compounds at high time resolution. Protonated oVOC, for example, can undergo dehydration, decarboxylation, and/or denitrification among other pathways, with differing and often unknown efficiencies for a given instrument, for example, ref 9. While such fragmentation from chemical ionization is still relatively minimal compared to electron impact ionization, quantification and attribution quickly becomes subject to significant uncertainties when applied to a complex matrix such as ambient air. The use of tandem mass spectrometry (MS-MS) can help identify structures of the dominant ions at a nominal mass-to-charge ratio and therefore partly address the presence of isobaric contaminant ions, but signal-to-noise limitations can prevent continuous application.[10,11]

Ion−molecule adduct formation is a chemical ionization pathway which provides the potential to achieve minimum fragmentation during ionization and thus preserve the parent

Received: January 21, 2014
Revised: April 25, 2014
Accepted: May 7, 2014
Published: May 7, 2014

molecule's composition. Adducts with iodide and bromide ions have formed an important approach in recent years to measuring molecular halogens and halogen oxide radicals using quadrupole mass spectrometers (QMS).[12−19] Ion adducts have also been applied to VOC measurements. Examples include the use of chloride (Cl^-) ions to detect carboxylic acids and aromatic chlorinated pesticides,[20,21] and more recently CF_3O^- to detect hydroxy hydroperoxides, peroxy acids and hydroxynitrates.[22−24] In laboratory settings, McNeill et al.[25] applied iodide-adducts to quantify carboxylic acids of atmospheric relevance with a QMS, although the propensity of Iodide to cluster with carboxylic acids had been known previously.[26] The Iodide-adduct QMS technique was also used by Le Breton et al.[27] to make airborne measurements of formic acid (CH_2O_2). And recently, adduct ionization utilizing $NO_3^-(HNO_3)_n$ and HSO_4^- ions was used to measure highly oxygenated organic molecules with a high-resolution time-of-flight chemical-ionization mass spectrometer (HR-ToF-CIMS).[28,29] Each of these various ion adduct approaches has a different selectivity toward VOC or inorganics.

Iodide (I^-) is significantly electronegative and a very weak gas-phase base. Electron transfer and proton abstraction are essentially negligible except for a few atmospherically relevant compounds, such as nitrate (NO_3) radicals in the case of charge transfer, and sulfuric acid (H_2SO_4) in the case of proton abstraction. Adduct formation is typically only slightly exoergic, and thus fragmentation is minimal. I^- also has a large mass-to-charge ratio (m/Q = 126.905 Th) and one of the largest negative mass defects, δ_m (= m/Q − round(m/Q)), among abundant natural elements (δ_m = −0.096 Th). Combined with the mass resolving power and mass accuracy of current commercially available field-deployable HR-ToF-MS instruments (Tofwerk AG, Aerodyne Research Inc.), > 5000 and <20 ppm (ppm), respectively,[30,31] the negative δ_m of Iodide provides an added degree of separation from other possible contaminant ions. This separation in turn provides greater selectivity and lower detection limits via higher signal at an exact m/Q relative to possible background signals caused by nonisobaric compounds at that nominal m/Q.

In this paper, we demonstrate the capabilities of HR-ToF-CIMS using Iodide-adduct ionization for the detection of oVOCs, and select inorganic gases such as nitrogen oxides, and illustrate its in-field performance using measurements made aboard the NOAA WP-3D aircraft during the Southeast Nexus (SENEX) campaign in June-July of 2013.

2. EXPERIMENTAL SECTION

The instrument used herein is similar to that described previously, consisting of a reduced-pressure ion−molecule reaction (IMR) region,[32−34] coupled to an atmospheric pressure interface HR-ToF-MS (Tofwerk AG, Thun, Switzerland).[30,31,35] A schematic is shown in the Supporting Information (SI) (Figure S1). As such, we briefly review updated components and focus on the Iodide-adduct HR-ToF-CIMS sensitivity to a suite of oVOCs and its deployment on an aircraft.

Ionization, Ion transmission, and Data Acquisition. A detailed schematic of the front-end interface between the aircraft sampling inlet and IMR is shown in the SI (Figure S2). Ambient air is drawn through a critical orifice at 2.0 standard liters per minute (slpm) into the IMR, which is held at 90 mbar by means of a scroll pump (Agilent IDP3) and a custom servo-controlled vacuum valve used to continuously regulate pumping speed. The pressure varies by <1% even as ambient pressure changes by factors of 5. The IMR temperature is controlled to within 0.2 °C at a set point between ambient and 40 °C depending upon application. Up to two commercial radioactive ion sources (Po-210, 10 mCi, NRD) oriented 90° apart and orthogonal to the ion−molecule reaction mixture flow can be used for switching between positive and negative reagent ions.[35] The IMR also contains a diffusion cell to continuously deliver calibration compounds for converting measured ion flight times into m/Q. As demonstrated below, Iodide-adduct ionization typically provides useful internal ions for calibrating the m/Q scale without the need for additional calibration compounds.

Iodide ions are generated by passing a 2 slpm flow of ultrahigh purity (UHP) N_2 over a permeation tube filled with methyl iodide and then through the Po-210 ion source into the IMR. The ionizer and sample flows mix and interact for ∼120 ms until a fraction is sampled through an orifice into a 4-stage differentially pumped chamber housing the HR-ToF-MS.[30] The first stage is held at 2 mbar by a molecular drag pump (Alcatel MDP 5011), and the second stage is held at 0.01 mbar by a split-flow turbo molecular pump (Pfeiffer). Two quadrupole ion guides transmit the ions through these two stages while providing collisional cooling and thus energetic homogenization of the ions as they enter the third "extractor" region. In the third and final stages, additional optics further focus the ions prior to being orthogonally pulsed at 22.22 kHz into the drift region where their arrival time after a V-mode trajectory is detected with a pair of microchannel plate detectors (Photonis Inc., U.S.A.).

The axial electric field strengths (<1 V/cm) in the first two stages are set to simultaneously optimize the total ion signal and the transmission of iodide-adducts. Optimization is obtained by maximizing the ratio of $I(H_2O)^-/I^-$ at a constant water vapor pressure in the IMR. It is possible to "tune" the selectivity of the instrument toward adducts with binding energies greater than that of $I(H_2O)^-/I^-$. Using previously determined thermodynamic values for iodide water monomer adducts,[7,8,36] it is clear that a significant fraction of these adducts are lost due to collision-induced declustering during transit from the IMR through the system (see SI).

The data acquisition procedures of this instrument have been described elsewhere in detail.[30,32] We have altered some aspects of this process for integration onto an aircraft. A standard laptop computer is used for instrument control and data acquisition, communicating with the acquisition and timing cards (AP240 and NI6320) via an external custom-built PCI box that allows data acquisition at ambient temperatures exceeding 40 °C. Additionally, at a chosen time interval (typically hourly) the temperature-dependent baseline of the AP240 acquisition card is determined in order to avoid unnecessarily rejecting small ion signals. The current version of the instrument, complete with pumps, draws <900 W of power, fits entirely within a 42 × 60 × 81 cm rack, and weighs 140 kg; it has been operated unattended for hours to days at a time in aircraft, ground-based trailers and on sampling towers.

In-Flight Sampling, Calibration and Background Determinations. Minimizing sampling losses of low volatility species is a priority. Ambient air is drawn at 22 slpm through a 72 cm long 1.6 cm inner diameter polytetrafluoroethylene (PTFE) tubing by a dedicated scroll pump (Agilent IDP3). The first 25 cm of the inlet tube is housed in an aerodynamic winglet that extends outside of the boundary layer of the WP-

3D aircraft (SI Figure S2). We estimate an inlet residence time of approximately 0.4 s at 1013 hPa while maintaining laminar flow (Re ~1900). A small fraction of the centerline flow (2 slpm) is sampled through a conical-shaped critical orifice into the IMR, while the remainder is exhausted through four radially symmetric ports located downstream and around the raised sampling orifice. The inlet is heated to 40 °C to minimize condensation on the tubing surface and to maintain a constant sampling environment under rapidly evolving outside and cabin conditions. Additional details are provided in the SI.

The instrument background signal is established by routinely introducing dry UHP N_2 directly in front of the critical orifice to displace the incoming ambient air. This addition is achieved by a servo-controlled, 7 cm (2.8 in.) long 0.3 cm (1/8 in.) diameter stainless steel probe that when actuated, enters from the side of the inlet at a 45° angle and is positioned directly upstream of, but not in contact with, the sampling cone. Ambient air is rejected from the IMR by overblowing the sampling orifice with N_2 (~3 slpm). When not in use, the probe is retracted so that it resides outside of the sample streamline (SI Figure S2). Traditional methods of scrubbing ambient air with a heated catalyst and/or chemical scrubbers were tested in the laboratory but lacked sufficient reproducibility and/or selectivity across the full m/Q scale to merit incorporation into short flight measurements. The humidity dependent partitioning of semivolatiles to surfaces is a confounding factor in the chosen approach. Instrument sensitivity dependence on water vapor pressure (discussed below) is accounted for, but given that the sensitivity for most organic compounds is higher in dry air, the measured background is more than likely an upper limit (SI Figure S3). UHP N_2 humidified to ambient levels will be used for background signal subtraction in future campaigns.

The stability of the instrument is determined by continuously delivering ^{13}C-labeled formic acid, $^{13}CH_2O_2$, through a 30 gauge 1.5 cm long needle bored through the PTFE inlet near the inlet entrance. The $^{13}CH_2O_2$ (Cambridge Isotopes) was contained in a custom-built PTFE permeation tube, held at constant temperature (40 °C) and pressure. The permeation rate was determined gravimetrically and compared to independently verified $^{12}CH_2O_2$ permeation tubes (KIN-TEK). Any drift in the instrument sensitivity measured by the $I(^{13}CH_2O_2)^-$ ion signal, not due to ambient water vapor (see below), is similarly applied to all other species using relative sensitivities which have been determined in the laboratory.

3. RESULTS AND DISCUSSION

General Spectrometer Performance and Mass Spectral Analysis. To introduce the ion chemistry and mass spectral analysis, an Iodide-adduct ionization spectrum observed during a SENEX flight is presented in Figure 1a. Iodide-adduct mass spectra contain several known single-ion peaks (e.g., I^-, IO^-, $I(H_2O)^-$, IO_2^-, $I(CH_2O_2)^-$, IO_3^-, $I(HNO_3)^-$, I_2^-, I_3^-), which are utilized to convert measured ion time-of-flight to mass-to-charge (m/Q, Th), and to determine the resolution and non-Gaussian ion peak shape using modified Toftools software from the University of Helsinki.[30] During SENEX, the absolute in-flight deviation of the assigned m/Q from their corresponding fitted curve is typically ±5 ppm (2σ), well within the manufacturer's stated mass accuracy of ±20 ppm.

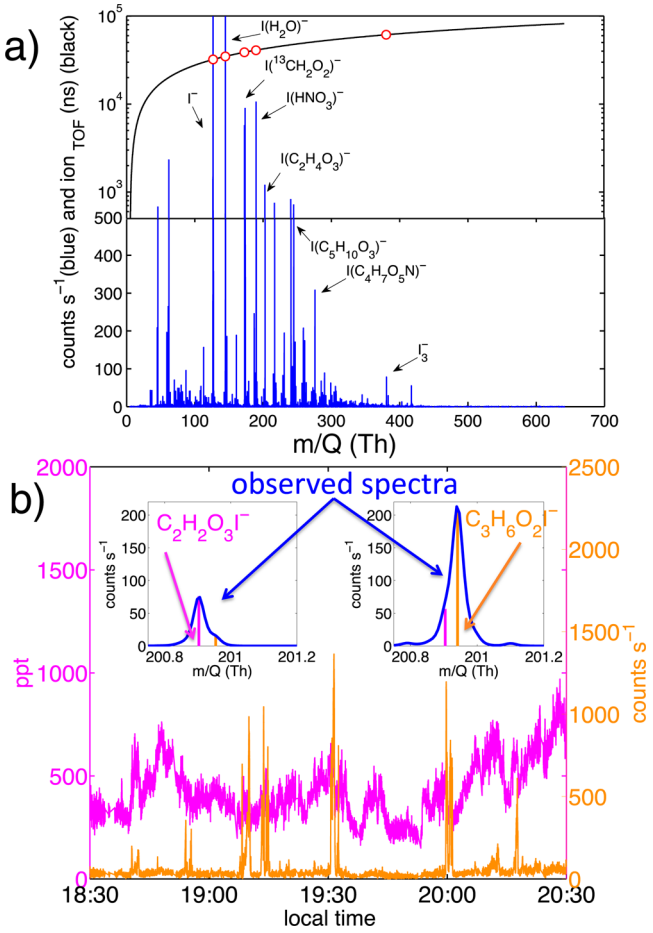

Figure 1. (a) A one-second averaged high-resolution mass spectrum (blue) observed in-flight during the SENEX 2013 campaign (lower portion), and the measured ion times of flight of known single ions (I^-, IH_2O^-, $^{13}CH_2O_2I^-$, $IHNO_3$) are plotted. The latter are used to determine the mass-to-charge (m/Q) for the rest of the spectrum (black). (b) Time series of $C_2H_2O_3I^-$ (magenta, left axis) and $C_3H_6O_2I^-$ (orange, right axis) observed on July 2 over Arkansas during SENEX. The high-resolution mass spectrum on the right inset is influenced by the presence of biomass burning tracers, while that on the left is not. At 1500 counts s^{-1}, the signal for $C_3H_6O_2I^-$ represents 340 ppt of propionic acid or 2.9 ppb of hydroxyacetone. Signal for $C_2H_2O_3I^-$ is attributed to glyoxylic acid.

The mass accuracy and resolving power can be used to separately quantify two compounds with the same nominal m/Q at high time-resolution. Figure 1b shows a time series and high-resolution mass spectra of ions with a nominal m/Q of 201 Th recorded during a nighttime flight over the Southeastern U.S. High resolution peak fitting requires two distinct ion compositions at that nominal m/Q: $I(C_2H_2O_3)^-$, the glyoxylic acid adduct, and $I(C_3H_6O_2)^-$, propionic acid or hydroxyacetone adducts. These two ion signals display dramatically different behavior as the aircraft flies through biomass burning plumes, illustrating the enhanced capability for attribution and detection provided by the instrument's mass resolving power and mass accuracy.

The above capabilities coupled to Iodide adduct ionization allow for additional insights into composition. Figure 2a contains the mass defect (δ_m) plotted versus the nominal m/Q of an Iodide ionization spectrum obtained during an α-pinene ozonolysis experiment using a steady state 0.75 m^3 PTFE chamber at the University of Washington (UW chamber). Ions

dx.doi.org/10.1021/es500362a | Environ. Sci. Technol. 2014, 48, 6309−6317

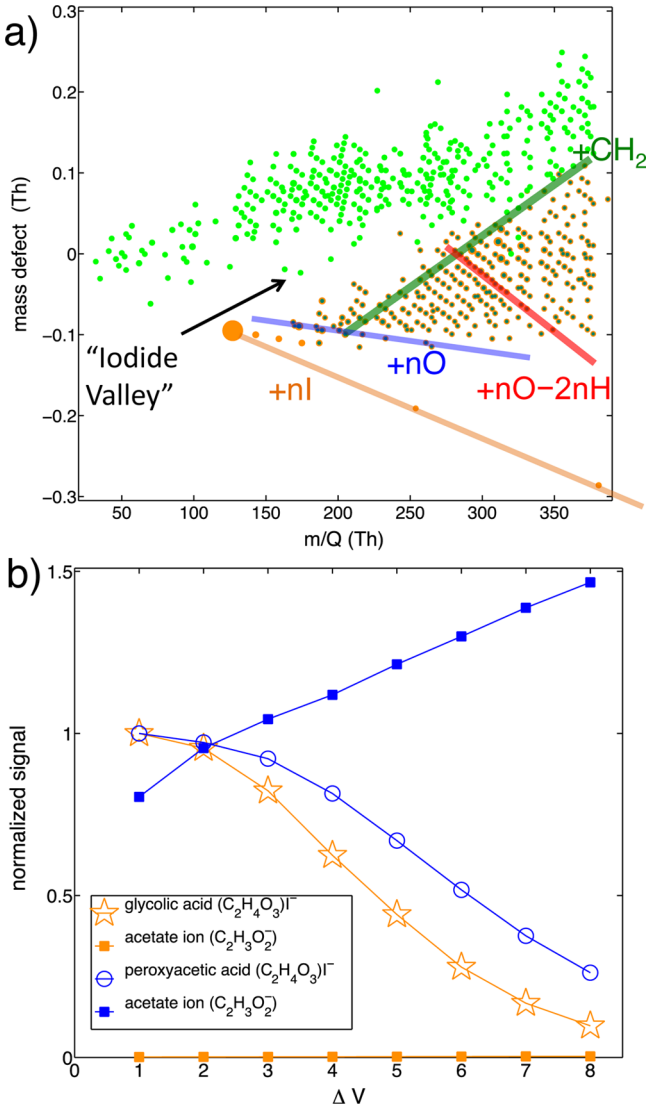

Figure 2. (a) High-resolution mass defect spectrum obtained during ozonolysis of α-pinene conducted in a 0.75 m^3 steady state PTFE chamber. The high mass-resolution and accuracy of the instrument allows ions containing Iodide (orange w/dark green) to be easily distinguished from those that do not (light green circles) due to the mass defect of Iodide. (b) Signals for the Iodide adducts, and the non-Iodide containing acetate ion, $C_2H_3O_2^-$, are plotted versus the voltage difference between the two quadrupoles regions (SI Figure S1) during additions of glycolic acid (gold stars and squares) and peroxyacetic acid (blue circles and squares). Raw signals are normalized to that of $(C_2H_4O_3)I^-$ at normal electric field settings ($\Delta V = 1$), and the voltage difference is referenced to that normally used. Note during peroxyacetic acid additions the presence of a large signal of the acetate ion, even at normal voltage settings. Both the rate at which the Iodide adduct ion is lost due to increasing the electric fields strengths, that is, declustering, and also the appearance of a fragment ion are ways in which varying these voltages can allow selectivity toward certain functional groups.

that contain Iodide (dark green with orange edge) generally have a negative or small positive δ_m, whereas those without (light green) have a positive δ_m, thereby creating an "Iodide Valley" separating compounds in m/Q space that cluster with Iodide from those that do not. Such additional information is not possible with charge transfer or proton transfer ionization schemes.

This space illustrates the multitude of byproducts observed during α-pinene ozonolysis. The δ_m of an ion increases with m/Q for each additional $-CH_2$ (Figure 2a, green line), whereas an additional oxygen atom yields a compound with a more negative δ_m (Figure 2a, red line). The row-like arrangement along the latter plane represents a loss of two hydrogen atoms for every oxygen atom added (gain of degree of unsaturation) for a given number of carbon atoms. Iodide-adduct ionization of a compound with a halogen atom will be shifted even further toward negative δ_m (Iodine more so than Bromine followed by Chlorine than Fluorine), a distinguishing feature of this class of compounds, suggesting that molecular halogen adducts with Iodide will be entirely separable in mass space from a range of possible interferences. This is evident in the δ_m versus m/Q plane associated with I^-, I_2^- and I_3^- (Figure 2a, orange line), the latter two of which are common but minor constituents of an Iodide-adduct ionization mass spectrum.

The compositions of organic anions lacking an Iodide (light green dots) typically involve an odd number of hydrogen atoms, at least 2 oxygen atoms and at least 1 degree of unsaturation, consistent with carboxylate anions. Additions of peroxyacetic acid (Sigma-Aldrich) and peroxypropionic acid (synthesized according to Phillips et al.[37]) yielded carboxylate signal levels that were comparable to that of the peroxyacid Iodide-adduct (Figure 2b). In contrast, additions of carboxylic acids, with a range of functionalities, never produced signal levels of the carboxylate anion above 0.1% of the corresponding Iodide-adduct. Indeed, scanning the electric field strength within the instrument induces decomposition of the peroxyacid-Iodide adducts into the corresponding carboxylate anion (Figure 2b), providing a potential means of identifying these isomers by both the persistence of the cluster ion (see also SI Figure S5) and the correlated appearance, or lack thereof, of product ions. Thus, many of the organic anions lacking an Iodide are likely from a reaction between I^- and peroxy acids, RC(O)OOH, as shown by Phillips et al.,[38] or other peroxides. Secondary ion chemistry involving, that is, proton abstraction ionization by acetate ions,[39] also cannot be ruled out. Regardless, this type of complexity encourages use of a "labeling" reagent ion such as Iodide-adducts to allow separation and/or identification of such processes.

Sensitivity to Oxygenated VOC. We have quantified the sensitivity of the Iodide-adduct HR-ToF-CIMS to several oVOCs and inorganic compounds. The response to a given compound is linear for atmospherically relevant concentrations (see SI Figures S6 and S7). In Table S1 (SI) and below we report sensitivities normalized to a million total reagent ion [I^- + $I(H_2O)^-$] counts per second (cps), which can vary from instrument to instrument and over time as the ion source degrades. These normalized sensitivity values depend on instrument parameters, including inlet and IMR temperature and pressures, and electric fields, which determine the m/Q transmission efficiency and declustering strength. Water vapor pressure can also affect sensitivities, as discussed in the next section. Consequently, the absolute values presented in SI Table S1 are specific to our instrument, which has been tuned to optimize the signal of $I(H_2O)^-$ (see SI), the thermodynamics of which are well understood (SI Figure S4).[7,8] The trends presented will likely be consistent between different instruments, assuming they are similarly optimized.

Calibrations are conducted using a range of methods. In one approach, a solution of the compounds is prepared at known concentrations in acetone (HPLC grade, Fischer Scientific).

dx.doi.org/10.1021/es500362a | Environ. Sci. Technol. 2014, 48, 6309−6317

Between 1 and 20 μL of the solution is injected onto a PTFE filter using a microliter syringe (Hamilton). The filter sits within a PTFE manifold 0.25 cm upstream of the critical orifice to the IMR. UHP N_2 gas that is continuously passed over the filter is slowly heated to 200 °C until the signal returns to preinjection levels. Integration of the signal and the mass injected allow a determination of the sensitivity. Injections are repeated several times to ensure repeatability, but may be biased low due to surface losses or degradation in solution. Calibration to very low volatility compounds is especially challenging given that thermal decomposition is possible prior to desorption from the filter,[40] and that Iodide-adducts are also subject to thermal decomposition at higher temperatures. The IMR on the current system is maintained at a constant temperature, so this latter effect is dampened, but both ultimately lead to lower limits to sensitivity values for compounds found predominantly in the condensed phase. A second approach uses calibrated permeation devices for formic, acetic, propionic, and nitric acids, the outputs of which were determined gravimetrically. The consistency between the solution injection and permeation device methods was confirmed by acetic, propionic and nitric acids for which both methods were possible. We also use a vapor pressure based delivery method, with catalytic conversion and subsequent optical measurement of carbon dioxide (CO_2) colocated at the inlet to the HR-ToF-CIMS (see SI).

The sensitivity of the Iodide-adduct HR-ToF-CIMS to a compound depends upon its polarity and hydrogen bonding capability, and is strongly influenced by molecular geometry and steric factors. The method is not sensitive to monoalcohols, monoketones or monoaldehydes, with sensitivity values falling below 0.1 cps $pptv^{-1}$, and is completely insensitive to nonoxygenated VOCs, due to their weak polarity and H-bonding, resulting in low binding energies with the I^-.[26,33] For organic compounds, a single acid group can provide the necessary binding energy to sensitively detect such compounds in the atmosphere, but an acid group is not required for high sensitivity. Sensitivity generally increases with the addition of a polar functional group such as keto-, hydroxy- and acid groups, in that order.

An example of sensitivity dependence on functional group is shown in Figure 3a for C_3 compounds (blue). The sensitivity to the monoacid (propionic acid, $C_3H_6O_2$), 6.6×10^{-2} counts s^{-1} ppt^{-1}, is less than that for the keto-monoacid (pyrvuvic acid, $C_3H_4O_3$), which is less sensitively detected than the hydroxy-monoacid (lactic acid, $C_3H_6O_3$) and diacid (malonic acid, $C_3H_4O_4$), 3.5×10^{-1}, 1.6 and 19 counts s^{-1} ppt^{-1}, respectively. The presence of a C═C double bond, as in the case of acrylic acid ($C_3H_4O_2$), compared to propionic acid does not appear to significantly alter the sensitivity. Moreover, though hydroxyacetone ($C_3H_6O_2$) and propionic acid are structural isomers, the former is not sensitively detected, 9.9×10^{-3} counts s^{-1} ppt^{-1}, consistent with carboxylic acids being better H-bonding donors than alcohols. In addition to the dependence on functional group, the sensitivity increases with mass-to-charge ratio, as shown in Figure 3a for monoacids (red) and keto-monoacids (cyan). This trend is attributed to the stability gained by the added vibrational modes over which to distribute excess energy for a larger molecule clustered to Iodide (see SI).

The enhancement in sensitivity provided by a second functional group is dependent on its location relative to the first. For instance, the instrument is particularly sensitive to specific isomers of isoprene hydroxy nitrate ($C_5H_9O_4N$),[41]

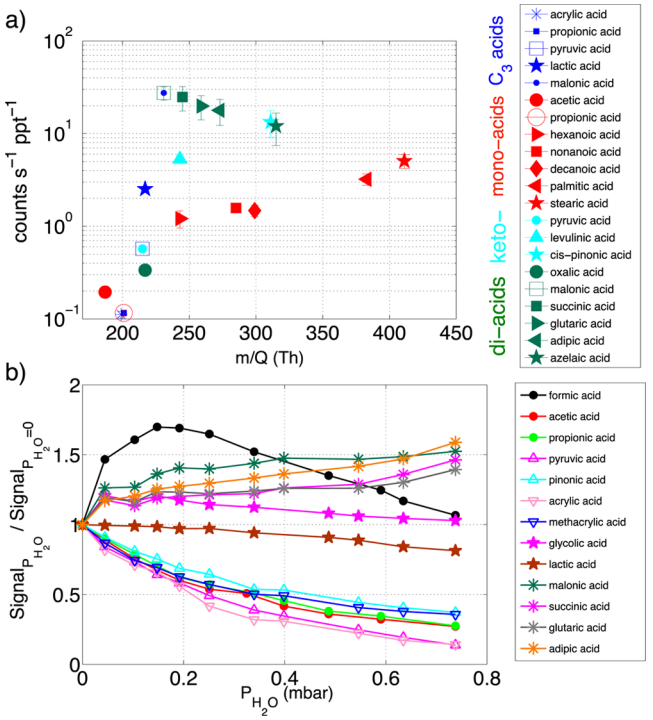

Figure 3. (a) Sensitivity (cps ppt^{-1}) per million total reagent ion cps at 0.25 mbar water vapor pressure for C_3 compounds (blue), monoacids (red), keto-monoacids (cyan), and diacids (green), plotted as a function of their m/Q (Th). Pyruvic acid, malonic acid and propionic acid are plotted twice, as they fall into two categories listed above. (b) Sensitivities of various oVOCs normalized to their respective values under dry conditions (P_{H2O} = 0, UHP N_2) as a function of water vapor pressure in the IMR.

namely, the β-4-hydroxy-3-nitrate and the *cis*-δ-1-hydroxy-4-nitrate. In contrast, it is not at all sensitive to the *trans*-δ-1-hydroxy-4-nitrate. These findings indicate that compounds containing hydroxyl and nitrate ($-ONO_2$) functional groups but without an acid group can be sensitively detected as Iodide adducts, but that both functional groups need to be accessible by Iodide to provide the necessary adduct stability required for efficient transmission to the time-of-flight region. In a similar way, though the instrument is minimally sensitive to most dihydroxy and diketo compounds, *cis*-2-butene-1,4-diol is an exception (SI Table S1), presumably due to the 1,4 placement of the two hydroxy groups and the *cis*- structure, which make the functional groups readily available to I^-.

The sensitivity to diacids (Figure 3a, green) is highest among all tested functional groups and is largely independent of m/Q. This feature is likely the result of the stability of the diacid Iodide-adduct allowing it to be transmitted through the system with minimal declustering. The observed sensitivity range of diacids is about 10 to 15% of the maximum allowable sensitivity, calculated assuming the adduct ions are formed at the kinetic limit with no subsequent losses. Not all diacids, however, are sensitively detected as an Iodide-adduct, as steric hindrance and geometry can affect the iodide-adduct reaction yield and/or the binding energy. Sensitivity to oxalic ($C_2H_2O_4$) and phthalic ($C_8H_6O_4$) acids is much lower than the other tested diacids, presumably due to the rigid structure and close proximity of the two hydroxy groups leading to H-bonding, thus limiting access to Iodide. Similarly, the sensitivity to methacrylic acid ($C_4H_6O_2$) is much lower than acrylic

dx.doi.org/10.1021/es500362a | Environ. Sci. Technol. 2014, 48, 6309−6317

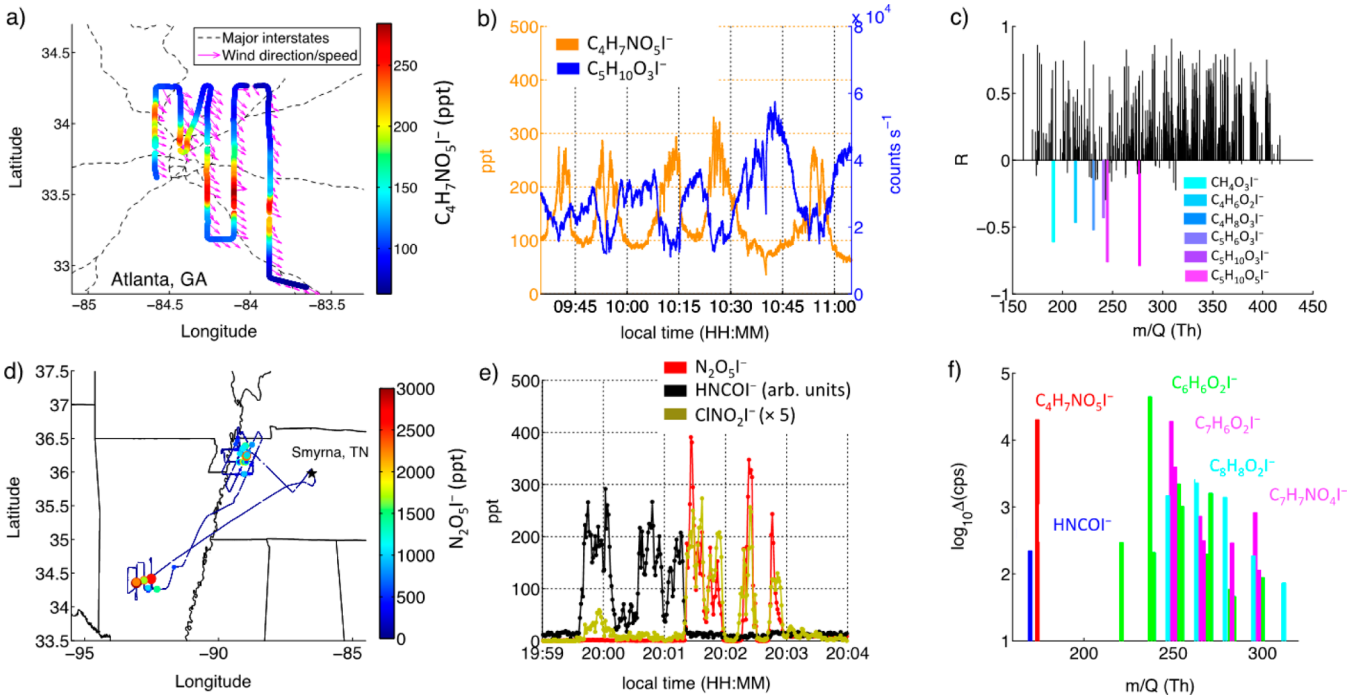

Figure 4. (a) Partial flight path over Atlanta, GA colored by $C_4H_7O_5NI^-$ mixing ratio obtained by applying the sensitivity of isoprene hydroxy nitrate, (b) time series of $C_4H_7O_5NI^-$ mixing ratio and $C_5H_{10}O_3I^-$ signals, and (c) the correlation spectrum with respect to $C_4H_7O_5NI^-$. Data presented in (a–c) correspond to observations made between 9:30 and 11:30 am local time on June 12 during the SENEX 2013 campaign. (d) Full flight path colored and sized by $N_2O_5I^-$ mixing ratio on the night of July 2–3 near the Tennessee, Arkansas and Missouri borders, (e) time series of $N_2O_5I^-$ and $ClNO_2I^-$ mixing ratios and the signal for $HNCOI^-$ (presumably isocyanic acid, a biomass burning tracer) on the same night, and (f) $\log_{10}$ of the median signal between 20:00 and 20:01 of select species enhanced with $HNCOI^-$. SI Figure S12 lists the full legend of the species in (f). The application of the isoprene hydroxy nitrate sensitivity to $C_4H_7O_5NI^-$ likely yields a low limit estimate on its mixing ratio.

$(C_3H_4O_2)$ and propionic $(C_3H_6O_2)$ acids, due likely to steric hindrance imparted by the $-CH_2$ or $-CH_3$ group adjacent to the carbonyl carbon.

The limit of detection for a given compound is determined by the signal (S) rate relative to the instrument background (B) count rate. Assuming the background count rate is the ion signal measured when the IMR inlet is overflowed with UHP N_2, we define the detection limit as the concentration which yields a S/B ratio of 3 in a 15-s integration time.[32] Corresponding average detection limits for a range of compounds measured during SENEX are listed in SI Table S1. For species with sensitivities >1 cps ppt^{-1}, detection limits are better than 17 ppt, and several are <1 ppt.

Determining the sensitivity to other functional groups and molecular structures is part of an ongoing effort. For example, SI Table S1 shows that the instrument is also highly sensitive to some inorganic acids and molecular halogen compounds, as expected from the previous work using QMS and iodide adduct ionization.[12,42] Moreover, it is plausible that manipulation of the electric fields used to transmit ions to the time-of-flight region, either in real time or prior to a measurement, can further enhance the selectivity of the instrument by utilizing differences in adduct binding energies (e.g., Figure 2b and SI Figure S5).

The Effect of Ambient Water Vapor on Ionization Efficiency. The efficiency of iodide-adduct ionization, and thus the inferred sensitivity, is affected by the presence of water vapor.[16,43] The sensitivity to a given compound will depend, in part, on whether water vapor competes with the Iodide ion, thereby lowering the sensitivity, or whether the presence of water vapor provides a third body to stabilize the Iodide-analyte cluster by carrying away excess energy from the collision, thereby increasing the sensitivity. Alternatively, if a compound forms a very stable complex with Iodide, and/or has enough internal vibrational modes to distribute excess energy from the collision complex, it may have an adduct formation efficiency that is independent of water vapor. While all of these possible effects are observed, we find the dominant effect of water vapor across the vast majority of organic compounds studied is to lower the sensitivity.

The I^- ion clustered with formic acid (CH_2O_2) is a good example of an adduct for which the competing influences of H_2O are exhibited, shown in Figure 3b (black). At low water vapor pressures in the IMR (P_{H2O}), the sensitivity to formic acid increases with increasing P_{H2O}, reaches maximum sensitivity around 0.2 mbar, then decreases with further increase in P_{H2O}. Computational results discussed in the SI indicate that reaction of CH_2O_2 with $I(H_2O)^-$ is less favorable than reaction with I^-. Therefore, the observed enhancing effect of water vapor pressure is a kinetic rather than a thermodynamic effect. That is, water molecules provide a third body to stabilize the Iodide-analyte cluster by distributing the excess energy over a greater number of vibrational modes, and carrying away excess energy from the ion–molecule collision leading to increased sensitivity, at least at low P_{H2O}. At high P_{H2O}, it appears that the kinetic enhancement is not enough to compensate for the additional competition of water for the Iodide ions, and $I(CH_2O_2)^-$ formation decreases with further increases in P_{H2O}.

We can estimate the maximum size of molecules for which enhancement of adduct formation by $I(H_2O)^-$ is important assuming binding energies and mean frequencies roughly

dx.doi.org/10.1021/es500362a | Environ. Sci. Technol. 2014, 48, 6309–6317

similar to those of $I(CH_2O_2)^-$. Using quantum Rice-Ramsberger-Kassel (QRRK) theory[44−46] we estimate ion−molecule cluster dissociation rates, which are strongly dependent upon the number of accessible vibrational modes (*s*) within the cluster (see SI). The predicted cluster decay rate becomes equal to the ion−molecule collision rate (at 90 mbar total pressure) for *s* of 8 to 9. Using the rule of thumb that *s* corresponds to half the total number of modes,[47] then molecules with 5 atoms or less will demonstrate an enhancement in Iodide adduct formation with increasing water vapor pressure, while molecules with >8 atoms will not do so (at least not for kinetic reasons).

Figure 3b presents experimental data consistent with the above theoretical guidelines. Using a dual-port inlet to minimize the effects of humidity dependent gas-surface partitioning (see SI), we find most oVOCs exhibit either a negative or negligible dependence on water vapor pressure. Diacids are the exception, the sensitivity to which tends to increase slightly with water vapor pressure for reasons yet to be determined. Molecular chlorine (Cl_2) and bromine (Br_2) exhibit increasing sensitivities as a function of water vapor pressure (SI Figure S8), as expected from the above. Containing 3 total atoms as adducts, the third-body effect due to the presence of water vapor outweighs the competition of water vapor for I^- over the range of P_{H2O} studied. Similar effects of water vapor have been reported for Iodide detection of other halogens and the peroxyacetyl radical, which have <8 atoms.[16,43] The water vapor pressure dependence for a range of other compounds detected as Iodide adducts is shown in SI Figures S9 and S10. The effect generally weakens as the atom number and oxygen and hydrogen content of the compound increases, consistent with an expected increase in the binding energy with Iodide for more polar compounds.

The HR-ToF-CIMS instrument has a continuous measure of water vapor in the ratio of $I(H_2O)^-/I^-$, see SI Figure S11, which can be used to account for changes in sensitivity when independent measures of water vapor are lacking (see SI). Moreover, continuous dilution with dry UHP N_2 or addition of water vapor to the ion source flow, can be used to suppress the actual vapor pressure of water in the IMR or the effects of atmospheric variability.

Applications to Studies of the Ambient Atmosphere. The I^- adduct HR-ToF-CIMS was deployed aboard the NOAA WP-3D aircraft as part of the Southeast Nexus (SENEX) campaign, based out of Smyrna, TN, during June and July of 2013. Boundary layer measurements in the Southeast U.S. were obtained over a span of nearly 125 flight hours under day and nighttime conditions, encountering a mixture of biogenic, urban, gas fields, power generation, and biomass burning emissions. The HR-ToF-CIMS provided simultaneous high-time resolution observations of a suite of oVOCs as well as select inorganic compounds.

Figure 4a shows part of the flight path colored by the mixing ratio of $C_4H_7O_5NI^-$ near Atlanta, GA (33.755°N, 84.390°W) on June 12th. An urban influence is clearly evident as the aircraft repeatedly intersects the Atlanta plume over and downwind of the city. The signal for $C_4H_7O_5NI^-$ increases within the urban plume−while the signal for a few others, notably $C_5H_{10}O_3I^-$, simultaneously decreases (Figure 4b). In the urban plume, which contains elevated levels of nitrogen oxides due to combustion, the dominant fate of organic peroxy radicals formed from the photo-oxidation of VOC such as isoprene will be reaction with nitric oxide (NO) to form organic nitrates and other products.[48,49] Outside the plume, the dominant fate will likely be formation of organic hydroperoxides from reaction with the hydroperoxy radical (HO_2).[24,50] Based on our sensitivity to functionalities discussed above, the C_4 and C_5 compounds shown in Figure 4 likely correspond to a hydroxy nitrate and hydroxy hydroperoxide or the derivative epoxide of isoprene. In addition to $C_5H_{10}O_3I^-$, the signals for only a few others (highlighted in Figure 4c) decrease within urban plumes, while most others increase. We have tentatively assigned elemental formulas for each ion peak shown in this spectrum. Sensitive and simultaneous detection of a suite of compounds in these rapidly changing chemical environments provides a comprehensive set of constraints on the cascade of oxidation products of biogenic VOCs, and the influence of anthropogenic emissions, temperature and sunlight.

Figure 4d shows the full flight path for a nighttime flight on July 2−3, colored and sized by the dinitrogen pentoxide, N_2O_5, mixing ratio measured with the instrument. In contrast to plumes emitted from cities (Figures 4a−c), those intercepted on this night are much narrower given their localized sources and weaker turbulent dispersion during nighttime. Figure 4e shows a brief time-series in which distinct plumes colocated in space but of different origin are sampled. A biomass burning plume−characterized by high levels of a phenolic compound, major constituents of biomass burning[35,51] − is sampled immediately before encountering a power plant plume−which due to its relatively high combustion efficiency is devoid of VOC but enriched in SO_x and NO_x. These conditions result in the production of N_2O_5 and subsequently nitryl chloride, $ClNO_2$, whereas in the VOC-rich biomass burning plumes the formation of N_2O_5 is presumably suppressed by the rapid reaction of its precursor, the nitrate radical, with VOCs. In addition to $C_7H_8O_2I^-$, the signal for numerous other C_6, C_7 and C_8 species are enhanced in these biomass burning plumes that have elemental formulas consistent with the presence of a phenyl group (Figure 4f).

The deployment on the NOAA WP-3D is the first for a HR-ToF-CIMS of its kind. These observations, though they represent only a subset of the data collected with this instrument during SENEX, illustrate the value of acquiring highly resolved mass spectra across a large m/Q range at high time-resolution when sampling a complex matrix such as ambient air where the type of compounds or locations that may be important are not necessarily known *a priori*. Using Iodide-adduct ionization we were able to detect a suite of aliphatic and aromatic oVOCs and alkyl nitrates derived from various directly emitted biogenic VOC (i.e., isoprene, 2-methyl-3-buten-2-ol, monoterpenes, etc.), as well as select inorganic species, all at the same time resolution (1 Hz), allowing for the characterization of air masses on small spatial scales from a rapidly moving platform. These capabilities will help determine the air quality and climate impacts of urban and industrial emissions in this region dominated by forests. To fully realize the potential of this instrument requires continued characterization and optimization of the selectivity and sensitivity of the Iodide-adduction ionization technique, for example, by utilizing differences in binding and/or reaction energies to allow separation of isomers containing different functional groups (see SI).

■ ASSOCIATED CONTENT

Supporting Information

Table S1 provides sensitivities and detection limits. Table S2 lists the energy values used in the Iodide water adduct simulation. Figure S1 shows the schematic of the HR-ToF-CIMS. Figure S2 is the layout of the inlet and chemical ionization interface used during the SENEX 2013 campaign. Figure S3 shows high-resolution mass spectra and time series during ambient and background measurements. Figure S4 compares the observed and modeled Iodide water adduct distribution. Figure S5 maps out the normalized signal for C_{10} nitrate compounds as a function of electric field strength. Figure S6 demonstrates the linearity of the instrument response to formic acid. Figure S7 is a formic acid versus nitric acid scatter plot during an experiment in which high levels of nitric acid was introduced. Figures S8−S10 illustrate the water vapor pressure dependence of the normalized sensitivities of selected compounds. Figure S11 compares IH_2O^-/I^- observed in the field versus in the laboratory. Figure S12 shows the complete legend for species presented in Figure 4f. Figure S13 shows inlet conditions during a typical SENEX campaign flight. Figure S14 shows the result of water vapor pressure correction on ^{13}C formic acid. This material is available free of charge via the Internet at http://pubs.acs.org/.

■ AUTHOR INFORMATION

Corresponding Author

*E-mail: thornton@atmos.uw.edu.

Author Contributions

⊥These two authors contributed equally to this manuscript

Notes

The authors declare no competing financial interest.

■ ACKNOWLEDGMENTS

We thank NOAA ESRL, especially J. A. de Gouw and C. Warneke, for accommodating our team during the SENEX 2013. In addition, we appreciate contributions from J. M. Roberts, J. A. Neuman, P. M. Edwards, P. Veres, and S. S. Brown of NOAA for useful discussions and providing us calibration standards in the field. The SENEX campaign would not have been possible without the patient help of the NOAA AOC personnel. We gratefully acknowledge L. Lee and R. C. Cohen of UC Berkeley for synthesizing hydroxy isoprene nitrates, and Y.-H. Lin and J. D. Surratt of UNC Chapel Hill for providing a sample of isoprene epoxydiol. We thank F. Rubach of Forschungszentrum Jülich for sharing the designs of his flight data acquisition system. We appreciate all of the contributions from the helpful personnel at Tofwerk AG, especially Christian Tanner, who implemented the online baseline correction function in the operating software. This work was supported by the U.S. Department of Energy SBIR (DE-SC0004577) and National Science Foundation (NSF CAREER ATM-0846183 to J.A.T.) programs. Funding for B. H. Lee was provided by the NOAA Climate & Global Change Postdoctoral Fellowship program.

■ REFERENCES

(1) Finlayson-Pitts, B. J. Halogens in the Troposphere. *Anal. Chem.* **2010**, *82* (3), 770−776.

(2) Heard, D. E. *Analytical Techniques for Atmospheric Measurement*; Blackwell Publishers: Oxford, Ames, IA, 2006; p xvii, 510 p., 4 p. of plates.

(3) Pratt, K. A.; Prather, K. A. Mass spectrometry of atmospheric aerosolsuRecent developments and applications. Part II: On-line mass spectrometry techniques. *Mass Spectrom Rev.* **2012**, *31* (1), 17−48.

(4) Finley, B. D.; Saltzman, E. S. Measurement of Cl_2 in coastal urban air. *Geophys. Res. Lett.* **2006**, *33*, 11.

(5) Goldstein, A. H.; Galbally, I. E. Known and unexplored organic constituents in the earth's atmosphere. *Environ. Sci. Technol.* **2007**, *41* (5), 1514−1521.

(6) Mao, J.; Ren, X.; Zhang, L.; Van Duin, D. M.; Cohen, R. C.; Park, J. H.; Goldstein, A. H.; Paulot, F.; Beaver, M. R.; Crounse, J. D.; Wennberg, P. O.; DiGangi, J. P.; Henry, S. B.; Keutsch, F. N.; Park, C.; Schade, G. W.; Wolfe, G. M.; Thornton, J. A.; Brune, W. H. Insights into hydroxyl measurements and atmospheric oxidation in a California forest. *Atmos Chem. Phys.* **2012**, *12* (17), 8009−8020.

(7) Caldwell, G.; Kebarle, P. Binding-energies and structural effects in halide anion ROH and RCOOH complexes from gas-phase equilibria measurements. *J. Am. Chem. Soc.* **1984**, *106* (4), 967−969.

(8) Caldwell, G. W.; Masucci, J. A.; Ikonomou, M. G. Negative-ion chemical ionization mass-spectrometry binding of molecules to bromide and iodide anions. *Org. Mass Spectrom* **1989**, *24* (1), 8−14.

(9) de Gouw, J.; Warneke, C. Measurements of volatile organic compounds in the earths atmosphere using proton-transfer-reaction mass spectrometry. *Mass Spectrom Rev.* **2007**, *26* (2), 223−257.

(10) Spicer, C. W.; Kenny, D. V.; Shaw, W. J.; Busness, K. M.; Chapman, E. G. A laboratory in the sky—New frontiers in measurements aloft. *Environ. Sci. Technol.* **1994**, *28* (9), A412−A420.

(11) St Clair, J. M.; McCabe, D. C.; Crounse, J. D.; Steiner, U.; Wennberg, P. O. Chemical ionization tandem mass spectrometer for the in situ measurement of methyl hydrogen peroxide. *Rev. Sci. Instrum.* **2010**, *81*, (9).

(12) Riedel, T. P.; Bertram, T. H.; Crisp, T. A.; Williams, E. J.; Lerner, B. M.; Vlasenko, A.; Li, S. M.; Gilman, J.; de Gouw, J.; Bon, D. M.; Wagner, N. L.; Brown, S. S.; Thornton, J. A. Nitryl chloride and molecular chlorine in the coastal marine boundary layer. *Environ. Sci. Technol.* **2012**, *46* (19), 10463−10470.

(13) Saltzman, E. S.; De Bruyn, W. J.; Lawler, M. J.; Marandino, C. A.; McCormick, C. A. A chemical ionization mass spectrometer for continuous underway shipboard analysis of dimethylsulfide in near-surface seawater. *Ocean Sci.* **2009**, *5* (4), 537−546.

(14) Thornton, J. A.; Kercher, J. P.; Riedel, T. P.; Wagner, N. L.; Cozic, J.; Holloway, J. S.; Dube, W. P.; Wolfe, G. M.; Quinn, P. K.; Middlebrook, A. M.; Alexander, B.; Brown, S. S. A large atomic chlorine source inferred from mid-continental reactive nitrogen chemistry. *Nature* **2010**, *464* (7286), 271−274.

(15) Chu, L. T.; Heron, J. W. Uptake of Hbr on ice at polar atmospheric conditions. *Geophys. Res. Lett.* **1995**, *22* (23), 3211−3214.

(16) Kercher, J. P.; Riedel, T. P.; Thornton, J. A. Chlorine activation by N_2O_5: Simultaneous, in situ detection of $ClNO_2$ and N_2O_5 by chemical ionization mass spectrometry. *Atmos. Meas. Tech.* **2009**, *2* (1), 193−204.

(17) Liao, J.; Sihler, H.; Huey, L. G.; Neuman, J. A.; Tanner, D. J.; Friess, U.; Platt, U.; Flocke, F. M.; Orlando, J. J.; Shepson, P. B.; Beine, H. J.; Weinheimer, A. J.; Sjostedt, S. J.; Nowak, J. B.; Knapp, D. J.; Staebler, R. M.; Zheng, W.; Sander, R.; Hall, S. R.; Ullmann, K. A comparison of Arctic BrO measurements by chemical ionization mass spectrometry and long path-differential optical absorption spectroscopy. *J. Geophys Res., Atmos* **2011**, 116.

(18) Mielke, L. H.; Furgeson, A.; Osthoff, H. D. Observation of $ClNO_2$ in a mid-continental urban environment. *Environ. Sci. Technol.* **2011**, *45* (20), 8889−8896.

(19) Osthoff, H. D.; Roberts, J. M.; Ravishankara, A. R.; Williams, E. J.; Lerner, B. M.; Sommariva, R.; Bates, T. S.; Coffman, D.; Quinn, P. K.; Dibb, J. E.; Stark, H.; Burkholder, J. B.; Talukdar, R. K.; Meagher, J.; Fehsenfeld, F. C.; Brown, S. S. High levels of nitryl chloride in the polluted subtropical marine boundary layer. *Nat. Geosci* **2008**, *1* (5), 324−328.

(20) Dougherty, R. C.; Roberts, J. D.; Biros, F. J. Positive and negative chemical ionization mass-spectra of some aromatic chlorinated pesticides. *Anal. Chem.* **1975**, *47* (1), 54−59.

(21) Tannenbaum, H. P.; Roberts, J. D.; Dougherty, R. C. Negative chemical ionization mass-spectrometry—Chloride attachment spectra. *Anal. Chem.* **1975**, *47* (1), 49−54.
(22) Beaver, M. R.; St Clair, J. M.; Paulot, F.; Spencer, K. M.; Crounse, J. D.; LaFranchi, B. W.; Min, K. E.; Pusede, S. E.; Wooldridge, P. J.; Schade, G. W.; Park, C.; Cohen, R. C.; Wennberg, P. O. Importance of biogenic precursors to the budget of organic nitrates: Observations of multifunctional organic nitrates by CIMS and TD-LIF during BEARPEX 2009. *Atmos. Chem. Phys.* **2012**, *12* (13), 5773−5785.
(23) Crounse, J. D.; McKinney, K. A.; Kwan, A. J.; Wennberg, P. O. Measurement of gas-phase hydroperoxides by chemical ionization mass spectrometry. *Anal. Chem.* **2006**, *78* (19), 6726−6732.
(24) Paulot, F.; Crounse, J. D.; Kjaergaard, H. G.; Kurten, A., St; Clair, J. M.; Seinfeld, J. H.; Wennberg, P. O. Unexpected epoxide formation in the gas-phase photooxidation of isoprene. *Science* **2009**, *325* (5941), 730−733.
(25) McNeill, V. F.; Wolfe, G. M.; Thornton, J. A. The oxidation of oleate in submicron aqueous salt aerosols: Evidence of a surface process. *J. Phys. Chem. A* **2007**, *111* (6), 1073−1083.
(26) Caldwell, G.; Renneboog, R.; Kebarle, P. Gas-phase acidities of aliphatic carboxylic-acids, based on measurements of proton-transfer equilibria. *Can. J. Chem.* **1989**, *67* (4), 611−618.
(27) Le Breton, M.; McGillen, M. R.; Muller, J. B. A.; Bacak, A.; Shallcross, D. E.; Xiao, P.; Huey, L. G.; Tanner, D.; Coe, H.; Percival, C. J. Airborne observations of formic acid using a chemical ionization mass spectrometer. *Atmos. Meas. Tech.* **2012**, *5* (12), 3029−3039.
(28) Ehn, M.; Kleist, E.; Junninen, H.; Petaja, T.; Lonn, G.; Schobesberger, S.; Dal Maso, M.; Trimborn, A.; Kulmala, M.; Worsnop, D. R.; Wahner, A.; Wildt, J.; Mentel, T. F. Gas phase formation of extremely oxidized pinene reaction products in chamber and ambient air. *Atmos. Chem. Phys.* **2012**, *12* (11), 5113−5127.
(29) Kulmala, M.; Kontkanen, J.; Junninen, H.; Lehtipalo, K.; Manninen, H. E.; Nieminen, T.; Petaja, T.; Sipila, M.; Schobesberger, S.; Rantala, P.; Franchin, A.; Jokinen, T.; Jarvinen, E.; Aijala, M.; Kangasluoma, J.; Hakala, J.; Aalto, P. P.; Paasonen, P.; Mikkila, J.; Vanhanen, J.; Aalto, J.; Hakola, H.; Makkonen, U.; Ruuskanen, T.; Mauldin, R. L.; Duplissy, J.; Vehkamaki, H.; Back, J.; Kortelainen, A.; Riipinen, I.; Kurten, T.; Johnston, M. V.; Smith, J. N.; Ehn, M.; Mentel, T. F.; Lehtinen, K. E. J.; Laaksonen, A.; Kerminen, V. M.; Worsnop, D. R. Direct observations of atmospheric aerosol nucleation. *Science* **2013**, *339* (6122), 943−946.
(30) Junninen, H.; Ehn, M.; Petaja, T.; Luosujarvi, L.; Kotiaho, T.; Kostiainen, R.; Rohner, U.; Gonin, M.; Fuhrer, K.; Kulmala, M.; Worsnop, D. R. A high-resolution mass spectrometer to measure atmospheric ion composition. *Atmos. Meas. Tech.* **2010**, *3* (4), 1039−1053.
(31) Yatavelli, R. L. N.; Lopez-Hilfiker, F.; Wargo, J. D.; Kimmel, J. R.; Cubison, M. J.; Bertram, T. H.; Jimenez, J. L.; Gonin, M.; Worsnop, D. R.; Thornton, J. A. A chemical ionization high-resolution time-of-flight mass spectrometer coupled to a micro orifice volatilization impactor (MOVI-HRToF-CIMS) for analysis of gas and particle-phase organic species. *Aerosol Sci. Technol.* **2012**, *46* (12), 1313−1327.
(32) Bertram, T. H.; Kimmel, J. R.; Crisp, T. A.; Ryder, O. S.; Yatavelli, R. L. N.; Thornton, J. A.; Cubison, M. J.; Gonin, M.; Worsnop, D. R. A field-deployable, chemical ionization time-of-flight mass spectrometer. *Atmos. Meas. Tech.* **2011**, *4* (7), 1471−1479.
(33) Yamdagni, R.; Kebarle, P. Intrinsic acidities of carboxylic-acids from gas-phase acid equilibria. *J. Am. Chem. Soc.* **1973**, *95* (12), 4050−4052.
(34) Aljawhary, D.; Lee, A. K. Y.; Abbatt, J. P. D. High-resolution chemical ionization mass spectrometry (ToF-CIMS): Application to study SOA composition and processing. *Atmos. Meas. Tech.* **2013**, *6* (11), 3211−3224.
(35) Mohr, C.; Lopez-Hilfiker, F. D.; Zotter, P.; Prevot, A. S. H.; Xu, L.; Ng, N. L.; Herndon, S. C.; Williams, L. R.; Franklin, J. P.; Zahniser, M. S.; Worsnop, D. R.; Knighton, W. B.; Aiken, A. C.; Gorkowski, K. J.; Dubey, M. K.; Allan, J. D.; Thornton, J. A. Contribution of nitrated phenols to wood burning brown carbon light absorption in Detling, United Kingdom during winter time. *Environ. Sci. Technol.* **2013**, *47* (12), 6316−6324.
(36) Lias, S. G., Bartmess, J. E.; Liebman, J. F.; Holmes, J. L.; Levin, R. D.; Mallard, W. G. Ion Energetics Data" in NIST Chemistry WebBook; *NIST Standard Reference Database 69*; Linstrom, P. J., Mallard, W. G., Eds.; National Institute of Standards and Technology: Gaithersburg, MD, http://webbook.nist.gov.
(37) Phillips, B.; Starcher, P. S.; Ash, B. D. Preparation of aliphatic peroxyacids. *J. Org. Chem.* **1958**, *23* (12), 1823−1826.
(38) Phillips, G. J.; Pouvesle, N.; Thieser, J.; Schuster, G.; Axinte, R.; Fischer, H.; Williams, J.; Lelieveld, J.; Crowley, J. N. Peroxyacetyl nitrate (PAN) and peroxyacetic acid (PAA) measurements by iodide chemical ionisation mass spectrometry: First analysis of results in the boreal forest and implications for the measurement of PAN fluxes. *Atmos. Chem. Phys.* **2013**, *13* (3), 1129−1139.
(39) Veres, P.; Roberts, J. M.; Warneke, C.; Welsh-Bon, D.; Zahniser, M.; Herndon, S.; Fall, R.; de Gouw, J. Development of negative-ion proton-transfer chemical-ionization mass spectrometry (NI-PT-CIMS) for the measurement of gas-phase organic acids in the atmosphere. *Int. J. Mass Spectrom.* **2008**, *274* (1−3), 48−55.
(40) Lopez-Hilfiker, F. D.; Mohr, C.; Ehn, M.; Rubach, F.; Kleist, E.; Wildt, J.; Mentel, T. F.; Lutz, A.; Hallquist, M.; Worsnop, D.; Thornton, J. A. A novel method for on-line analysis of gas and particle composition: Description and evaluation of a Filter Inlet for Gases and AEROsols (FIGAERO). *Atmos. Meas. Technol.* **2014**, *7* (4), 983−1001, DOI: 10.5194/amt-7-983-2014.
(41) Lee, L.; Teng, A. P.; Wennberg, P. O.; Crounse, J. D.; Cohen, R. C. On rates and mechanisms of OH and O_3 reactions with isoprene-derived hydroxy nitrates. *J. Phys. Chem. A* **2014**, *118* (9), 1622−1637.
(42) Wolfe, G. M.; Thornton, J. A.; Yatavelli, R. L. N.; Mckay, M.; Goldstein, A. H.; LaFranchi, B.; Min, K. E.; Cohen, R. C. Eddy covariance fluxes of acyl peroxy nitrates (PAN, PPN and MPAN) above a Ponderosa pine forest. *Atmos, Chem. Phys.* **2009**, *9* (2), 615−634.
(43) Slusher, D. L.; Huey, L. G.; Tanner, D. J.; Flocke, F. M.; Roberts, J. M. A thermal dissociation-chemical ionization mass spectrometry (TD-CIMS) technique for the simultaneous measurement of peroxyacyl nitrates and dinitrogen pentoxide. *J. Geophys Res., Atmos.* **2004**, *109*, D19.
(44) Dean, A. M. Predictions of pressure and temperature effects upon radical-addition and recombination reactions. *J. Phys. Chem.* **1985**, *89* (21), 4600−4608.
(45) Kassel, L. S. Studies in homogeneous gas reactions II Introduction of quantum theory. *J. Phys. Chem-Us* **1928**, *32*, 1065−1079.
(46) Rice, O. K.; Ramsperger, H. C. Theories of unimolecular gas reactions at low pressures. *J. Am. Chem. Soc.* **1927**, *49*, 1617−1629.
(47) Laidler, K. J. *Chemical Kinetics*, 3rd ed.; Harper & Row: New York, 1987; p xi, 531 p.
(48) Paulot, F.; Crounse, J. D.; Kjaergaard, H. G.; Kroll, J. H.; Seinfeld, J. H.; Wennberg, P. O. Isoprene photooxidation: New insights into the production of acids and organic nitrates. *Atmos. Chem. Phys.* **2009**, *9* (4), 1479−1501.
(49) Horowitz, L. W.; Liang, J. Y.; Gardner, G. M.; Jacob, D. J. Export of reactive nitrogen from North America during summertime: Sensitivity to hydrocarbon chemistry. *J. Geophys. Res., Atmos.* **1998**, *103* (D11), 13451−13476.
(50) Crutzen, P. J.; Williams, J.; Poschl, U.; Hoor, P.; Fischer, H.; Warneke, C.; Holzinger, R.; Hansel, A.; Lindinger, W.; Scheeren, B.; Lelieveld, J. High spatial and temporal resolution measurements of primary organics and their oxidation products over the tropical forests of Surinam. *Atmos. Environ.* **2000**, *34* (8), 1161−1165.
(51) Yee, L. D.; Kautzman, K. E.; Loza, C. L.; Schilling, K. A.; Coggon, M. M.; Chhabra, P. S.; Chan, M. N.; Chan, A. W. H.; Hersey, S. P.; Crounse, J. D.; Wennberg, P. O.; Flagan, R. C.; Seinfeld, J. H. Secondary organic aerosol formation from biomass burning intermediates: Phenol and methoxyphenols. *Atmos. Chem. Phys.* **2013**, *13* (16), 8019−8043.